Effect of ebullition and groundwater temperature on estimated dinitrogen excess in contrasting agricultural environments

Article *in* Science of The Total Environment · July 2019

DOI: 10.1016/j.scitotenv.2019.133638

CITATIONS
3

READS
68

6 authors, including:

Micòl Mastrocicco
Università degli Studi della Campania "Luigi Vanvitelli
226 PUBLICATIONS **1,884** CITATIONS
SEE PROFILE

Elisa Soana
University of Ferrara
48 PUBLICATIONS **745** CITATIONS
SEE PROFILE

Nicolò Colombani
Università Politecnica delle Marche
215 PUBLICATIONS **1,912** CITATIONS
SEE PROFILE

Simona Castaldi
Università degli Studi della Campania "Luigi Vanvitelli" (previous Second Universi…
106 PUBLICATIONS **5,813** CITATIONS
SEE PROFILE

Effect of ebullition and groundwater temperature on estimated dinitrogen excess in contrasting agricultural environments

Micol Mastrocicco[1], Elisa Soana[2], Nicolò Colombani[3#], Fabio Vincenzi[2], Simona Castaldi[1], Giuseppe Castaldelli[2]

[1]DiSTABiF - Department of Environmental, Biological and Pharmaceutical Sciences and Technologies, Campania University "Luigi Vanvitelli", Via Vivaldi 43, 81100 Caserta, Italy

[2]SVeB - Department of Life Sciences and Biotechnology, University of Ferrara, Via L. Borsari 46, 44121 Ferrara, Italy

[3]SIMAU - Department of Materials, Environmental Sciences and Urban Planning, Polytechnic University of Marche, Via Brecce Bianche 12, 60131 Ancona, Italy

[#]Corresponding author: Dr. Nicolò Colombani (n.colombani@univpm.it)

Abstract

Denitrification is a key microbial-mediated reaction buffering the impact of agriculturally-derived nitrate loads. Groundwater denitrification capacity is often assessed by measuring the magnitude and patterns of dinitrogen excess, although this method can be biased by dissolved gasses exsolution and ebullition. To address this issue, shallow groundwater was sampled in two field sites via nested mini-wells on a monthly basis over an entire hydrological year and analysed for dissolved gasses, nitrate and physical parameters. Both sites are located in lowland areas of the Po River basin (Italy) and are characterized by intensive agriculture. The GUA site, a freshwater paleo-river environment, with a low content of organic matter (SOM) and oxic sub-oxic groundwater. The

BAN site, a reclaimed brackish swamp environment, with abundant SOM and sulphidic-methanogenic groundwater. Groundwater samples evidenced a general deficit of dinitrogen and Argon concentrations, because of ebullition induced by a total dissolved gasses pressure exceeding the hydrostatic pressure. Ebullition was recorded only during winter at the reclaimed brackish soil and was triggered by methane exsolution. While in summer both sites were affected by ebullition because of the water table drawdown. Denitrification evaluated using dinitrogen excess via dinitrogen-Argon ratio technique, was not only affected by gas exsolution, but also by groundwater temperature fluctuations. In fact, the latter induced large biases in the calculated N_2 excess even in the freshwater paleo-river environment. For these reasons, dinitrogen excess estimate with standard methods resulted to be unreliable in both lowland environments and a modified method is here presented to overcome this issue.

Keywords

Dissolved gasses, denitrification, exsolution, groundwater temperature, gas partial pressure.

1. Introduction

In terrestrial ecosystems, denitrification, the microbial anaerobic respiration leading to reduction of nitrate (NO_3^-) or nitrite (NO_2^-) to gaseous N oxides and molecular N_2, is frequently occurring in water saturated soils rich in SOM (Taylor and Townsend, 2010) and in particular of labile organic substrates which provide electron donors (Castaldelli et al., 2019; Castaldelli et al., 2013). These soils are easily characterized by hypoxic conditions and are most typical of poorly drained lowland environments (Vepraskas, 2015). Where lowland areas are used for agriculture only extensive ditching allows to increase the drainage to the point of creating suitable conditions for root growth of crops (Ward et al., 2018). In hydric soils of agricultural lands, denitrification can be measured in relatively shallow groundwater at significant depths below the rooting zone (Anderson et al., 2014; Starr and Gillham, 1993; Tesoriero et al., 2000), although at higher depth the lower availability of

organic substrates might represent a limiting factor for denitrification activity (Chen et al., 2018; Mastrocicco et al., 2011b). At landscape level, the spatial and temporal variability of denitrification rates is mainly dependent on the soil texture, the agricultural practices and climatic factors (Aguilera et al., 2013; Barakat et al., 2016). However, where agricultural soils are characterized by shallow aquifers, the seasonal trend of denitrification activity and the key drivers of such trends are not yet accurately characterized.

Reduced gaseous compounds like N_2, CO_2, H_2S and CH_4 are among the main products of anaerobic decomposition of organic matter, which is carried out by many different facultative and obliged anaerobic microorganisms, including denitrifiers (Anderson et al., 2014; Rivett et al., 2008). The general order of production in anaerobic conditions is generally following the Gibbs free energy (Chapelle et al., 1995): N_2 from denitrification, CO_2 from manganese and iron reduction, H_2S from sulphate reduction, CH_4 from CO_2 reduction and/or acetate fermentation. These gasses usually accumulate in groundwater along the soil profile and might be degassed into the atmosphere at significant rates when the water table drops, as the reduction of in pore pressure lowers dissolved gasses solubility and results in exsolution (Fortuin and Willemsen, 2005). Then, the total gas pressure may increase above the hydrostatic pressure and the vertical transport of gas bubbles driven by buoyancy forces may occur. This phenomenon, known as ebullition (Amos and Mayer, 2006), can have important implications on gas transport to the atmosphere from aquifers and within the aquifer and the unsaturated zone.

Denitrification capacity in groundwater is often assessed by measuring the magnitude and patterns of groundwater N_2 excess, i.e. biogenic N_2 water concentration, in excess of atmospheric equilibrium (Denver et al., 2014; Fox et al., 2014; Vogel et al., 1981; Weymann et al., 2008). Since now the approach followed to calculate N_2 excess is to use a constant groundwater temperature, but this assumption is hardly verified when the water table is shallow (Colombani et al., 2016a; Kurylik et al., 2014). Moreover, there is not clear evidence if this approach can be considered reliable over an entire hydrological year or might pose problems of interpretation when the water table

fluctuations and the consequent changes in dissolved gas partial pressure alter the gas/groundwater equilibrium.

To fill this knowledge gap, dissolved gasses were monitored monthly during a whole hydrological year in two areas characterized by soils with contrasting textures and content of SOM. The main objectives of the study were: i) to verify whether denitrification can be accurately estimated in shallow aquifers of agricultural soils by simply monitoring N_2 excess; ii) to evaluate the influence of key environmental parameters like temperature, water table elevation, biogeochemical conditions and reactions, on the variability of dissolved gasses concentration in groundwater.

2. Material and Methods

2.1. Study sites

The two field sites are located in the Po Delta, the lowest territory of the Po River watershed (5 m to -3 m a.s.l.). The GUA site, located at 44°47”42’N and 11°42”22’ E (Fig. 1), pertains to a freshwater paleo-river environment characterized by a moderately alkaline silty-loam soil (Hypocalcic Haplic Calcisols), with upper horizons characterized by silty clay loamy texture and lower horizons by calcareous silty loamy texture. The BAN site, located at 44°39”32’N and 11°52”14’ E (Fig. 1), is part of a reclaimed brackish swamp area, characterized by a silty-clay soil (Calcaric Gleyic Cambisols), moderately alkaline, with silty clay or clay loamy textures and peaty lenses at depths of 2.0-2.5 m below ground level (b.g.l.).

Both sites are cultivated with a rotation of wheat and maize, while only occasionally with beetroot and sorghum. Each site receives a N fertilization based on NPK mineral fertilizers, NH_4NO_3 and/or synthetic urea, in different combinations and for a total amount of about 160 kg N/ha/y and 240 kg N/ha/y, for wheat and maize respectively. These rates are lower than most of the intensive agricultural cultivations in Northern Italy, since this area is classified as vulnerable to NO_3^- following the enactment of the European Water Framework Directive (2000/60/CE). In November 2016 both sites were equipped with a series (4 replicates) of multi-level samplers (MLS), i.e. three

PVC nested mini-wells with an internal diameter of 2 cm, filled in the last 20 cm with a 50 µm Nitex mesh, placed just below the maximum water table elevation and at -1 m and -2 m below the latter.

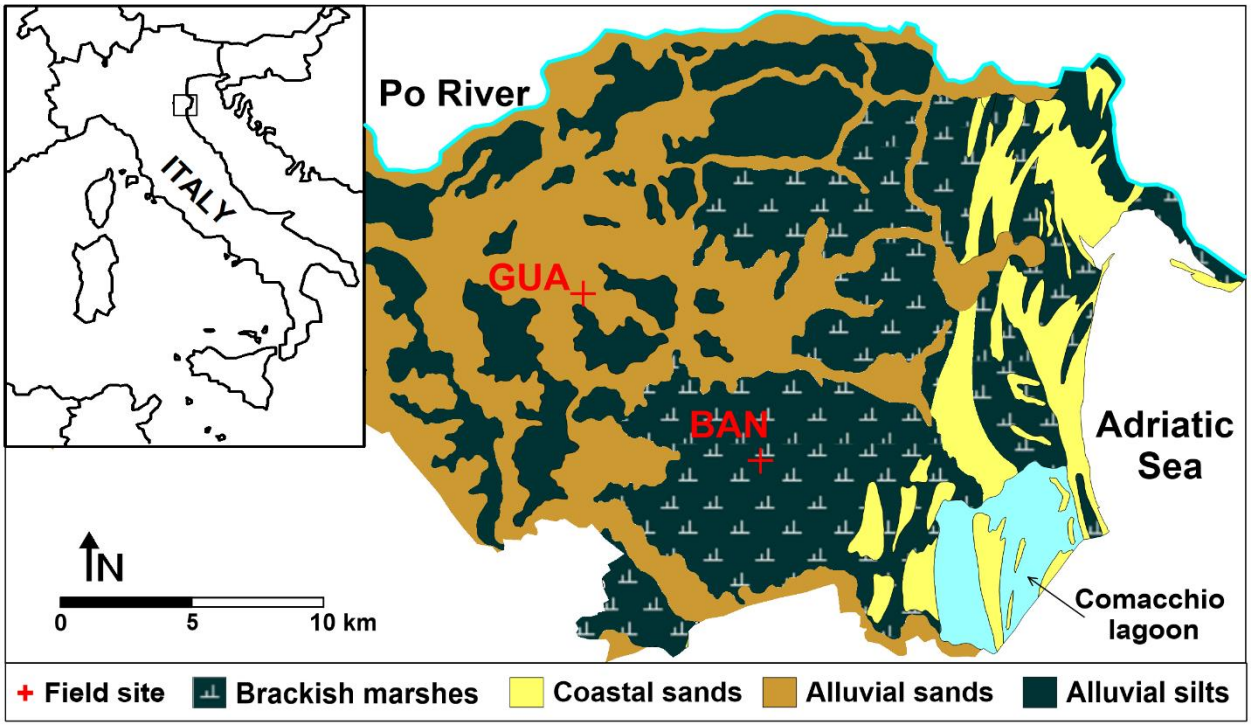
ITALY
Po River
GUA
BAN
Adriatic Sea
Comacchio lagoon
N
0
5
10 km
+ Field site
Brackish marshes
Coastal sands
Alluvial sands
Alluvial silts

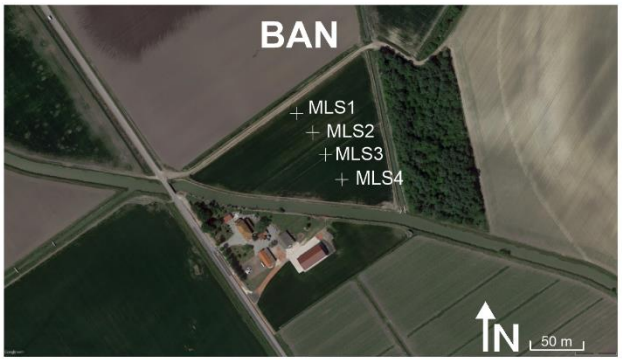
BAN
MLS1
MLS2
MLS3
MLS4
N
50 m

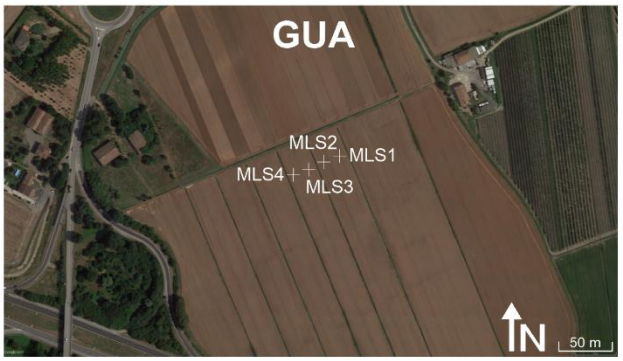
GUA
MLS2
MLS1
MLS4
MLS3
N
50 m

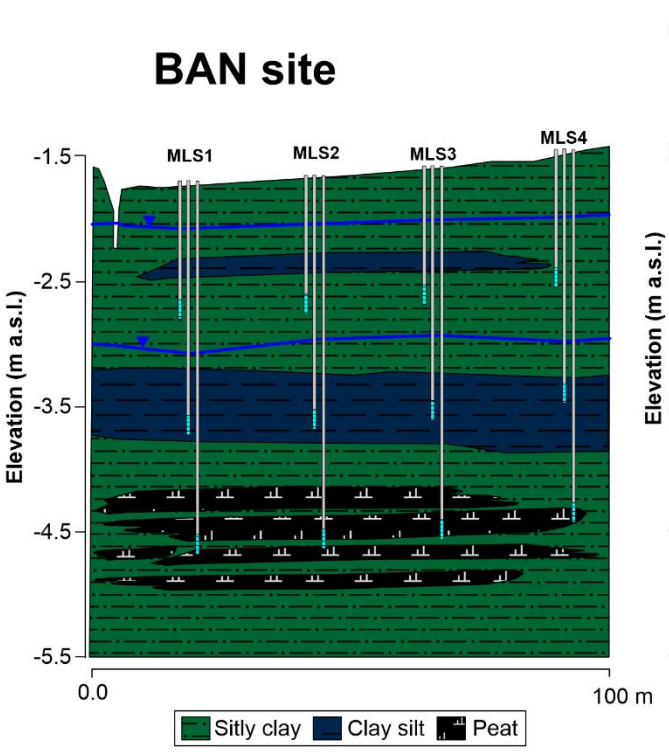
BAN site
MLS1
MLS2
MLS3
MLS4
-1.5
-2.5
-3.5
-4.5
-5.5
Elevation (m a.s.l.)
0.0
100 m
Sitly clay
Clay silt
Peat

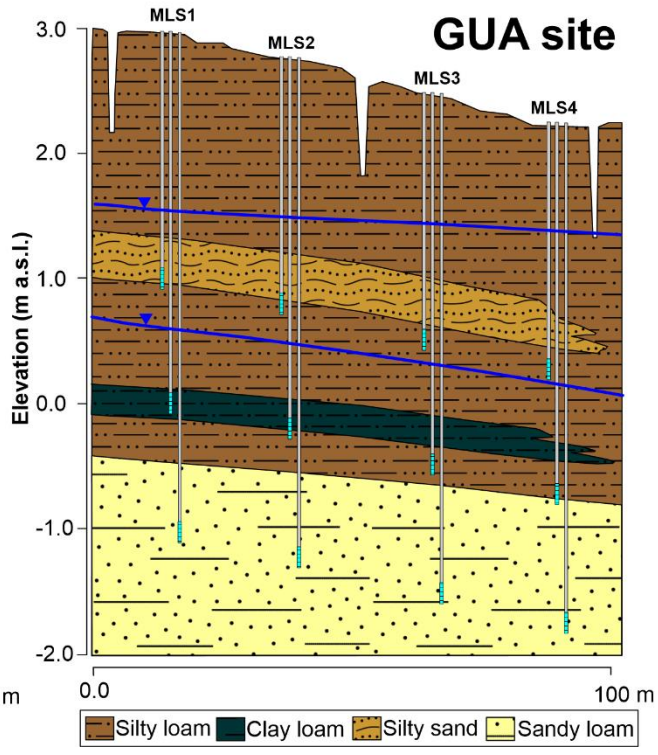
GUA site
MLS1
MLS2
MLS3
MLS4
3.0
2.0
1.0
0.0
-1.0
-2.0
Elevation (m a.s.l.)
0.0
100 m
Silty loam
Clay loam
Silty sand
Sandy loam

107

Figure 1: The upper panel shows the location of the two field sites with their soil texture. The middle panel shows the satellite images of both sites with the location of MLSs. The lower panel shows the hydrogeological profiles along the MLSs' location, the major lenses and the minimum and maximum water table position during the monitoring period (blue lines).

The sites were selected since they are representative of the most common environments of the Po River lowland with more than 60% of the territory covered by these soil textures (Mastrocicco et al., 2010). The area, which accounts for more than 1000 km^2, has been intensively cultivated since the last century because of its flat topography and the large surface water availability. Despite many information existing on the most important hydrogeological mechanisms regulating the aquifers and microbial processes affecting NO_3^- fate and transport in groundwater (Caschetto et al., 2017; Mastrocicco et al., 2017; Mastrocicco et al., 2011a; Sacchi et al., 2013), there is still a limited comprehension of the role of denitrification in attenuating NO_3^- pollution in these shallow aquifers.

2.2. Sampling and analytical methods

Groundwater samples were collected from the MLS monthly, over an entire hydrological year starting from 10 January 2017. Groundwater sampling was performed with a low flow inertial pump to avoid dissolved gasses stripping. At all sampling events, temperature, electric conductivity (EC), dissolved oxygen, pH and oxygen reduction potential (ORP) were also measured using a portable HANNA Instr. Probes.

To estimate the hydraulic conductivity (*K*) variability, slug tests were performed in all the piezometers with a pneumatic initiation system to instantaneously lower the static groundwater level of approximately 0.5 m. All the acquired slug test responses were analysed using the Bouwer and Rice method (Bouwer and Rice, 1976). The hydrostatic pressure at the screened depth of each piezometer was calculated from the pressure head (meters of water column above the piezometer screen, which was converted into barometric pressure).

A total of 185 samples were analysed for dissolved N_2, Ar, CO_2, H_2S, CH_4. Samples for Ar, N_2 and CH_4 determinations were collected by overflowing at least 3 times 12-mL gas-tight glass vials (Exetainer®, Labco, High Wycombe, UK) and preserved by adding 100 µL of 7M $ZnCl_2$ solution. Water samples were analysed at the laboratory of Aquatic Ecology, University of Ferrara, by MIMS-Membrane Inlet Mass Spectrometry (Bay Instruments, USA; Kana et al., 1994), a PrismaPlus quadrupole mass spectrometer with an inline furnace operating at 600°C to allow for O_2 removal. The CH_4, N_2 and Ar concentrations were quantified by the ion current detected at m/z ratios of 15, 28, and 40, respectively. The primary standard for MIMS analyses is de-ionized water maintained at a constant temperature (20°C) in a circulating bath with headspace at 100% relative humidity and equilibrated to atmospheric gasses by low stirring. The ion currents were standardized by applying the gas solubility equations of Weiss (1970) and the instrument drift was corrected by measuring thermally equilibrated water every six samples. Due to the very low concentration in air, a separate standard procedure for CH_4 was used following the headspace equilibration technique. Standards were prepared by injecting known amounts of pure gas (>99.0%, Sigma Aldrich) into the headspace of 12-mL gas-tight glass vials filled with de-ionized water. Prior to MIMS analyses, the vials were shaken vigorously for a minute and placed in a thermostatic bath for solubility equilibration.

Total alkalinity was measured titrimetrically with 0.1 eq/L HCl (Anderson et al., 1986) in a 5 mL sub-aliquot of groundwater samples kept frozen until analysed. Dissolved CO_2 concentrations were calculated via PHREEQC-3 (Parkhurst and Appelo, 2013) using measured alkalinity, ionic strength, pH and temperature of each groundwater sample. Dissolved HS^- was measured spectrophotometrically on a double beam Jasco V-550 spectrophotometer (Cline, 1969) in a 5 mL sub-aliquot of groundwater samples kept frozen until analysed.

The gas concentration (µmol/L) was transformed into partial pressure according to Henry's law:

$$p_x = \frac{c_x}{s_x} \quad (1)$$

where p_x is the partial pressure of gas x (atm), C_x is the concentration of gas x (µmol/L) and S_x is the solubility of gas x when x is the only gas present, at 1 atm. total pressure. The Bunsen coefficient for each gas species was determined at any given temperature and salinity, following Colt (2012).

2.3. N_2 excess calculation methods

Dissolved N_2 in groundwater consists of atmospheric N_2 plus N_2 from denitrification (excess N_2) accumulated during the groundwater flow path (Böhlke, 2002) or from other processes like pyrite oxidation via NO_3^- reduction and anammox-anaerobic NH_4^+ oxidation (Rivett et al., 2008). N_2 from denitrification or other NO_3^- reduction processes can be calculated by subtracting atmospheric N_2 from total N_2 (N_{2Tot}). Atmospheric N_2 in groundwater consists of equilibrium solubility of N_2 and N_2 from "excess air" (Aeschbach-Hertig et al., 2008).

The first method to calculate excess N_2 (N_{2Exc}M1) uses the following equation (Weymann et al., 2008):

$$N_{2Exc}M1 = N_{2Tot} - N_{2EA} - N_{2EQ} \quad (2)$$

where N_{2Tot} represents the measured molar concentration of the total dissolved N_2 in groundwater and N_{2EQ} is the molar concentration of dissolved N_2 in equilibrium with the atmospheric concentration. For the equilibrium temperature, a constant value of 13°C was assumed which was the mean measured groundwater temperature over the monitoring period, N_{2EQ} was thus obtained using N_2 solubility data (Weiss, 1970). In addition to a constant temperature value, the equation 2 was computed using temperatures recorded in the field for each groundwater sample. N_{2EA} denotes N_2 from excess air, which is the dissolved N_2 gas component originating from the entrapment of air bubbles near the water table during recharge (Holocher et al., 2002).

For a given recharge temperature, excess air is usually back calculated using several noble gas concentrations (Cey et al., 2009; Holocher et al., 2002). Although, data on dissolved noble gasses are usually difficult to obtain without extremely specialized analytical equipment (Klump et al., 2008). In this study the procedure proposed by Weymann et alii (2008) was followed to calculate

185 the minimum and maximum values of N_{2EA} using only Ar as noble gas. Thus, the lowest and upper
186 estimates of N_{2EA} were used to assess the uncertainty of our excess N_{2Exc} estimates connected with
187 excess air fractionation at each site. Ar was selected as tracer since is present in air at well
188 measurable concentrations being the third-most abundant gas in the Earth's atmosphere (about 0.9%
189 v/v, after N_2 and O_2). It has approximately the same solubility in water as O_2 and is more soluble in
190 water than N_2. Moreover, MIMS has maximum resolution at mass generally below 45 and thus Ar
191 falls exactly where resolution is thehighest. A second method (M2), modified from Blicher-
192 Mathiesen et alii (1998) was also applied to have another estimate of the N_{2Exc}. Briefly, the method
193 allows to calculate the amount of N_2 degassed (N_{2Deg}) and the excess N_2 (N_{2Exc}M2) via the following
194 equations:

195 $$N_{2Deg} = N_{2Tot} \frac{\left({}^{N_{2Atm}}/_{N_{2EQ}}\right)}{\left({}^{Ar_{Atm}}/_{Ar_{EQ}}\right)} \ln\left(\frac{Ar_{EQ}}{Ar_{Tot}}\right) \quad (3)$$

196 $$N_{2Exc}M2 = \left(N_{2Tot} + N_{2Deg}\right) - N_{2EQ} \quad (4)$$

197 where Ar_{Atm} is the volumetric fraction of Ar in the atmosphere with saturated air and N_{2Atm} is the
198 volumetric fraction of N_2 in the atmosphere with saturated air. Ar_{EQ} is the groundwater dissolved Ar
199 concentration in equilibrium with the atmosphere at the sediment temperature at a given piezometer,
200 Ar_{Tot} is the measured groundwater dissolved Ar concentration at a given piezometer.
201

202 ## 3. Results and discussion

203 ### 3.1. Water table, temperature and electrical conductivity fluctuations

204 The water table in both sites showed clear seasonal fluctuation with two recharging events
205 occurring in winter and spring and a marked drawdown in summer (Fig. 2 upper panels). The latter
206 was driven by evapotranspiration, that is quite pronounced in the area during the crop growing
207 season (i.e. from April to September).

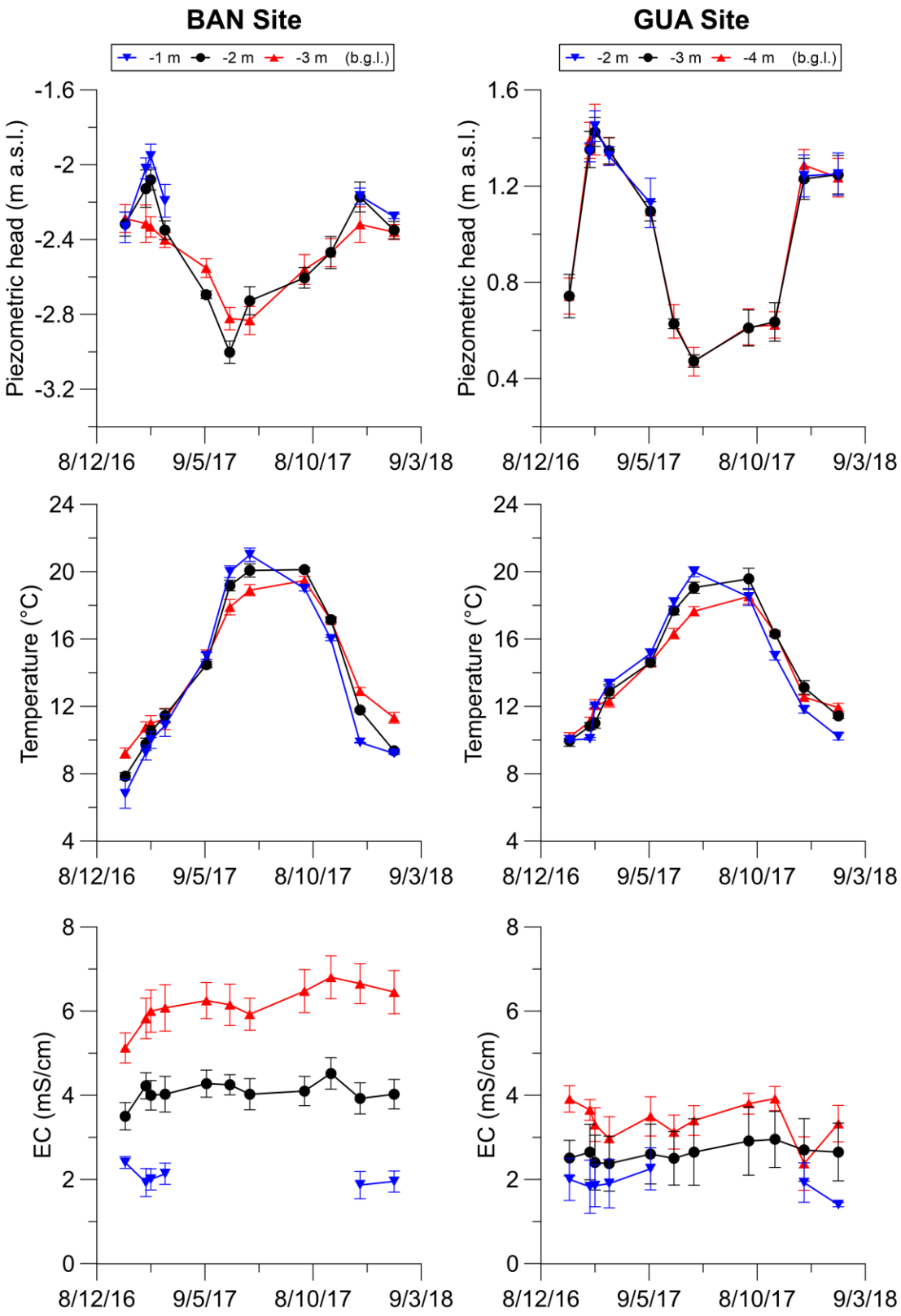

Figure 2: Piezometric heads (upper panels), temperature values (middle panels) and EC values (lower panels) recorded in the MLSs at the two sites. The error bars represent the standard deviation over 4 replicate plots.

In this period, characterized by high temperatures (max, min, average) which favour both crop transpiration and evaporation, the water table is near the ground surface and soils are characterized by an elevated capillary rise (Colombani et al., 2016b; Mastrocicco et al., 2010).

Both GUA and BAN sites hosted an unconfined aquifer superimposed to a confined aquifer, indeed the piezometers showed different head values at different depths at a given date (Fig. 1, 2). This is due to the relatively thick and continuous clay and silt lens present at BAN at approximately -3.5 m a.s.l. and by a clay-loam lens at GUA located at approximately 0.0 m a.s.l. that also affect the vertical distribution of the hydraulic conductivity (Table 1). The clay and silt lens therefore, can be considered aquitards which locally impede vertical groundwater fluxes and gasses migration.

Table 1. *K* values (± 1 st.dev, n=4) measured in the two sites at different depths.

Piezometer depth (m b.g.l.)	***K* value (m/s)**
-1 at BAN	$6.3*10^{-7}$ ($\pm 4.1*10^{-7}$)
-2 at BAN	$2.2*10^{-7}$ ($\pm 1.0*10^{-7}$)
-3 at BAN	$3.1*10^{-6}$ ($\pm 1.7*10^{-6}$)
-2 at GUA	$8.9*10^{-6}$ ($\pm 1.2*10^{-6}$)
-3 at GUA	$2.7*10^{-7}$ ($\pm 5.2*10^{-7}$)
-4 at GUA	$3.6*10^{-5}$ ($\pm 3.1*10^{-6}$)

It could be noticed that the degree of confinement is higher at BAN than at GUA since the thickness of the low permeability lens is higher at BAN and in addition at GUA the lens is also thinning over the right corner of the monitored transect (Fig. 1). The seasonal trend of the temperatures recorded at different depths in the MLS is similar in both sites (Fig. 2, middle panels) but in BAN the minimum and maximum values are lower and higher than in GUA, respectively. This might be explained by a shorter water table depth respect to the ground surface in BAN compared to GUA

231 (Fig. 1, lowest panels). The smaller standard deviation of the recorded temperatures respect to the
232 standard deviation of the recorded piezometric heads, suggests a uniform redistribution of
233 temperature's gradients with respect to the depth from the ground surface. Finally, the EC is similar
234 in both sites at the shallowest depth, while at deeper depth EC at BAN is much higher than at GUA
235 (Fig. 2, lower panels). This could be explained by the brackish paleo-marshes present in BAN.
236 These environments are quite widespread in the shallow coastal aquifers of the Po River lowland
237 (Castaldelli et al., 2013; Greggio et al., 2018). In terms of temporal variability, there was no clear
238 seasonal pattern in the EC values at both sites. Besides, the high EC standard deviation suggests a
239 large heterogeneity of chemical composition of the infiltrating waters, affected by preferential flow
240 paths and local changes of the hydraulic conductivity field (Mastrocicco et al., 2011b).
241
242 **3.2. Dissolved gasses in groundwater**
243 Figure 3 shows the observed dissolved Ar and N_2 concentrations in groundwater compared to the
244 theoretical gasses' solubility in water in equilibrium with the atmosphere at a given salinity (0.5 to
245 5.3 g/L) and temperature (from 5 to 25°C, covering the seasonal range detected *in situ*). Most of the
246 groundwater samples collected in the lowest piezometer (-3 m b.g.l.) at BAN lie on the left side of
247 the red line. A deficit in dissolved N_2 and Ar concentrations with respect to the theoretical values
248 predicted for water temperature higher than 25°C indicates a possible ebullition of groundwater
249 samples. Differently, all other samples from BAN lie close on the equilibrium line but slightly on
250 the right side. At GUA a less wide range of both Ar and N_2 concentrations is found, with only a few
251 samples lying on the left side of the red line, while most of the samples are slightly enriched in N_2.
252 This evidence could indicate denitrification processes acting in the middle piezometers (-3 m b.g.l.)
253 and in some samples from the lower piezometers (-4 m b.g.l.).
254 To better elucidate the role of CH_4 in driving the dissolved N_2 concentrations, a scatter diagram is
255 shown in Figure 4 for both sites. A relationship is found linking the decrease of dissolved N_2
256 concentrations with the exponential increase of CH_4 in groundwater sampled in the peaty layer (-3

m b.g.l. at BAN; Fig. 1, lower panel). Although the R^2 is not elevated, it is undeniable that increasing CH_4 in groundwater lead to a decrease of N_2. As a comparison, the same exponential relationship was applied to data from GUA with extremely poor results (R^2 close to 0; Fig. 4). In GUA, the concentration of CH_4 was always extremely low, possibly due to the lack of SOM that did not support extremely reducing conditions favourable to methanogenesis (Table 2). On the contrary, the presence of a peat layer below the piezometer at -3 m b.g.l. in the BAN might have favoured methanogenesis and consequently CH_4 exsolution leading to the occurrence of ebullition causing N_2 degassing. At GUA these conditions were most probably never met and N_2 potentially could accumulate.

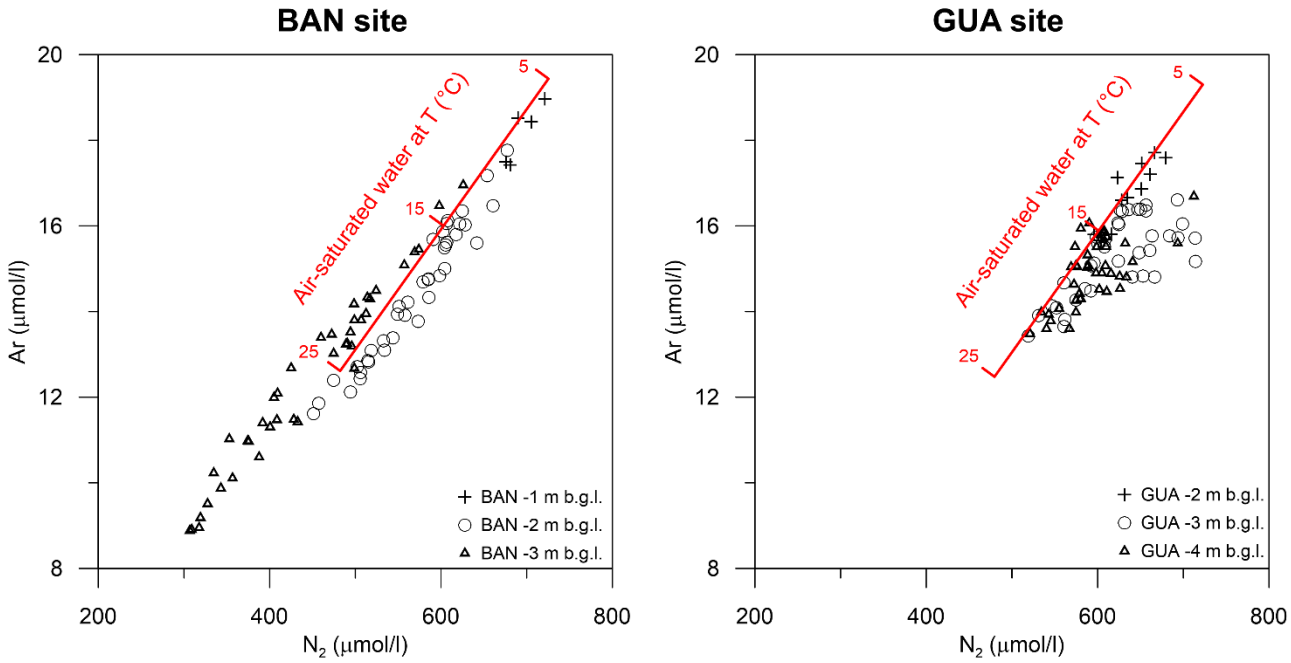

Figure 3: Dissolved Ar versus dissolved N_2 in groundwater at BAN and GUA sites. The red line represents the Ar and N_2 concentrations in air-saturated water at different temperatures (red numbers indicate the temperature values).

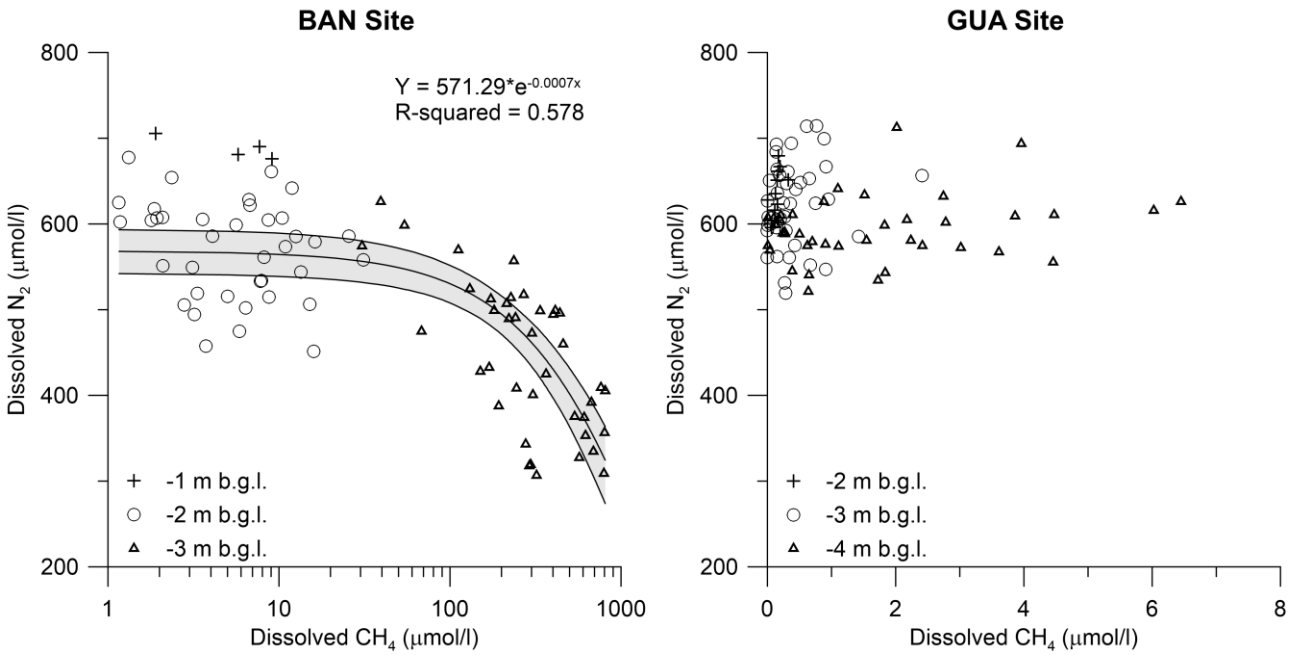

Figure 4: Dissolved N_2 versus dissolved CH_4 in BAN and GUA sites. The black line represents the best fit with an exponential law ($p<0.05$) and the grey shaded area is the 95% confidence interval.

3.3. N_{2Exc} calculation and comparison

In figure 5 the comparison between the maximum and minimum expected N_{2Exc} values using only Ar as noble gas to determine the excess air is shown. It can be noticed that at BAN the relationship between the two calculated N_{2Exc} values is extremely poor, with a Pearson correlation coefficient (r) of -0.132. On the other hand, GUA shows a better relationship between the two calculated N_{2Exc}, with a Pearson correlation coefficient of 0.642. Despite of this, the uncertainties connected with the calculated N_{2Exc} values are still too elevated to be considered acceptable. In fact, Weymann et alii (2008) presented N_{2Exc} data which were much closer to the 1:1 line than the ones presented here.

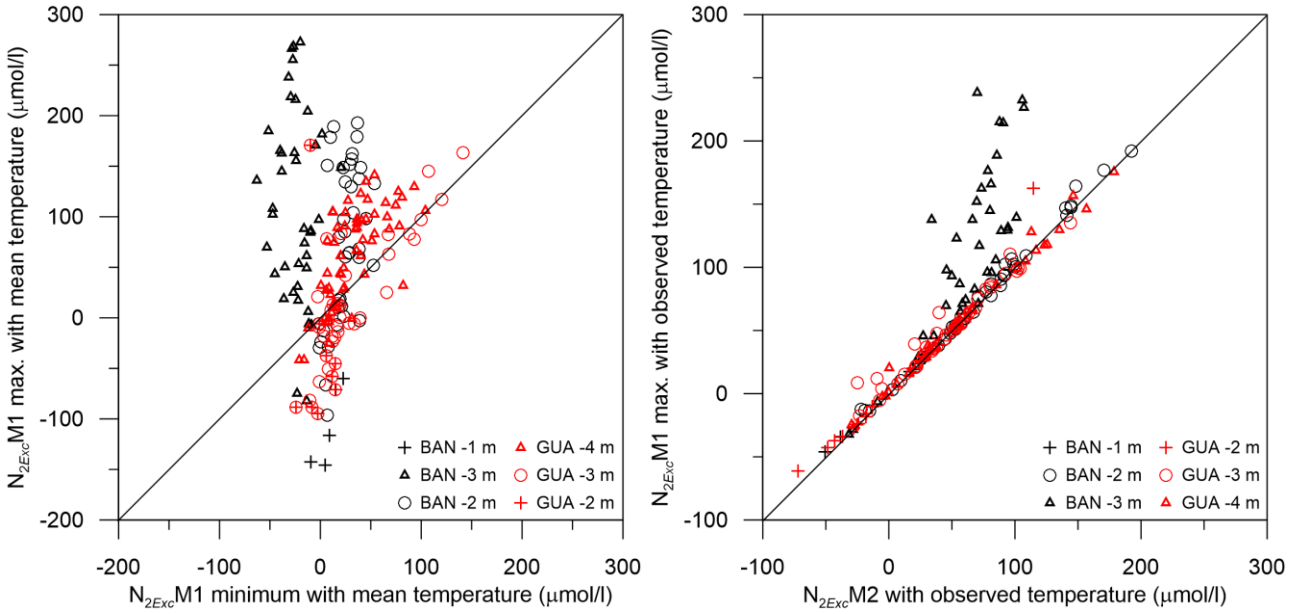

Figure 5: The left panel shows the N_{2Exc}M1 calculated using the maximum physically based values at the mean temperature versus N_{2Exc}M1 calculated using the minimum physically based values at the mean temperature in both BAN and GUA sites. The right panel shows the N_{2Exc}M1 calculated using the maximum physically based values at the observed temperature versus N_{2Exc}M2 calculated using the mean physically based values at the observed temperature. The black line represents the 1:1 fit line for which the two methods M1 and M2 would attain a perfect agreement.

The right panel of figure 5 shows that a very good *r* value (0.986) is found for GUA between the N_{2Exc}M1 maximum values calculated using the observed temperatures and the N_{2Exc}M2 values calculated with the modified Blicher-Mathiesen et alii (2002) method (M2). For BAN a lower *r* value is found (0.811), but it must be stressed that the samples which fall outside the 1:1 line are only the -3 m b.g.l. ones, which also have the highest CH_4 dissolved concentrations leading to exsolution. In fact, excluding the -3 m b.g.l. samples an *r* value of 0.997 is found, which is even higher than the one found in GUA. The samples collected at -3 m b.g.l. have extremely high CH_4 concentrations, as shown in Figure 4. Thus, CH_4 exsolution might cause the anomalous results of N_{2Exc} at BAN -3 m b.g.l., as frequently reported in the literature (Amos and Mayer, 2006; Fortuin and Willemsen, 2005). Various attempts to compare the Weymann et alii (2008) method (M1)

303 calculated with observed temperatures instead of mean recharge temperature and M2 method failed
304 to produce *r* values above 0.5, thus the results are not shown.
305 A possible explanation of the good fit between the method M1 and M2 is that the assumption of
306 local equilibrium between the water and gas phases is appropriate at both the investigated sites. In
307 fact, the assumption at the base of the N_{2Exc}M1 maximum values is that if excess air results from
308 complete dissolution of gas bubbles in groundwater, the excess air gas composition is identical to
309 atmospheric air composition (Aeschbach-Hertig et al., 2008). As pointed out by Klump et alii
310 (2008), groundwater table fluctuations in temperate climate zones are usually within the range of a
311 few meters, and the thickness of the quasi-saturated zone is therefore limited. Under these
312 conditions, flow velocities of 10 m/d or larger would require a kinetic fractionation approach for gas
313 dissolution, to accurately account for incomplete dissolution of entrapped gas bubbles. Whereas,
314 kinetic fractionation could be neglected for velocities smaller than 1 m/d (Klump et al., 2008), and
315 thus for low flow velocities sites as the investigated ones. Moreover, it must be remarked that the
316 temperature effect is the major driver of gasses solubility in shallow groundwater, while salinity
317 only slightly affect the effective gasses solubility in the studied environments that are freshwater or
318 brackish (Colt, 2012; Fortuin and Willemsen, 2005).
319 The modified method of Blicher-Mathiesen et alii (2002) seems a good approach to correctly
320 evaluate the N_{2Exc} in shallow aquifers pertaining to lowland agricultural environments when CH_4
321 dissolved concentrations are below 100 µmol/l. To further proof if this concept can be considered
322 robust, the following section describes a comparison between hydrostatic head pressures and
323 dissolved gasses partial pressures.
324

325 **3.4. Comparison between hydrostatic heads and dissolved gasses partial pressures**

326 Figure 6 depicts the comparison between the partial pressures of dissolved gasses and the
327 hydrostatic pressures at BAN and GUA sites during the summer and winter sampling campaigns.
328 Although, not measured in this study, dissolved N_2O was considered to have a negligible effect on

329 gas pressure given that the concentrations found in these soils are very low (Castaldelli et al., 2019)
330 and that in highly reducing conditions N_2O tends to be reduced completely to N_2. The hydrostatic
331 pressures at BAN in winter were higher than the total pressure of dissolved gases in the upper and
332 medium piezometers, while in the lower ones oversaturation with gasses was apparent and thus a
333 significant gas loss would be expected in the lower part of the aquifer. The total gas pressure was
334 prevalently formed by N_2, but CH_4 was the one that contributed chiefly to exceed the hydrostatic
335 pressure at the peaty lenses' location (-3 m b.g.l.).
336 The hydrostatic pressures at GUA in winter were found to be higher than the total pressure of
337 dissolved gasses in all the MLS, witnessing that groundwater was undersaturated with gasses and
338 no significant gas loss would be expected. But if this is valid for the recharge season, it does not
339 hold true during the summer season, where the water table drawdown drastically decreases the
340 hydrostatic head pressure. In fact, at both BAN and GUA sites the total gas pressure highly
341 exceeded the hydrostatic head pressure in all the MLS triggering ebullition processes. Although, the
342 gasses responsible for such processes were different from site to site.

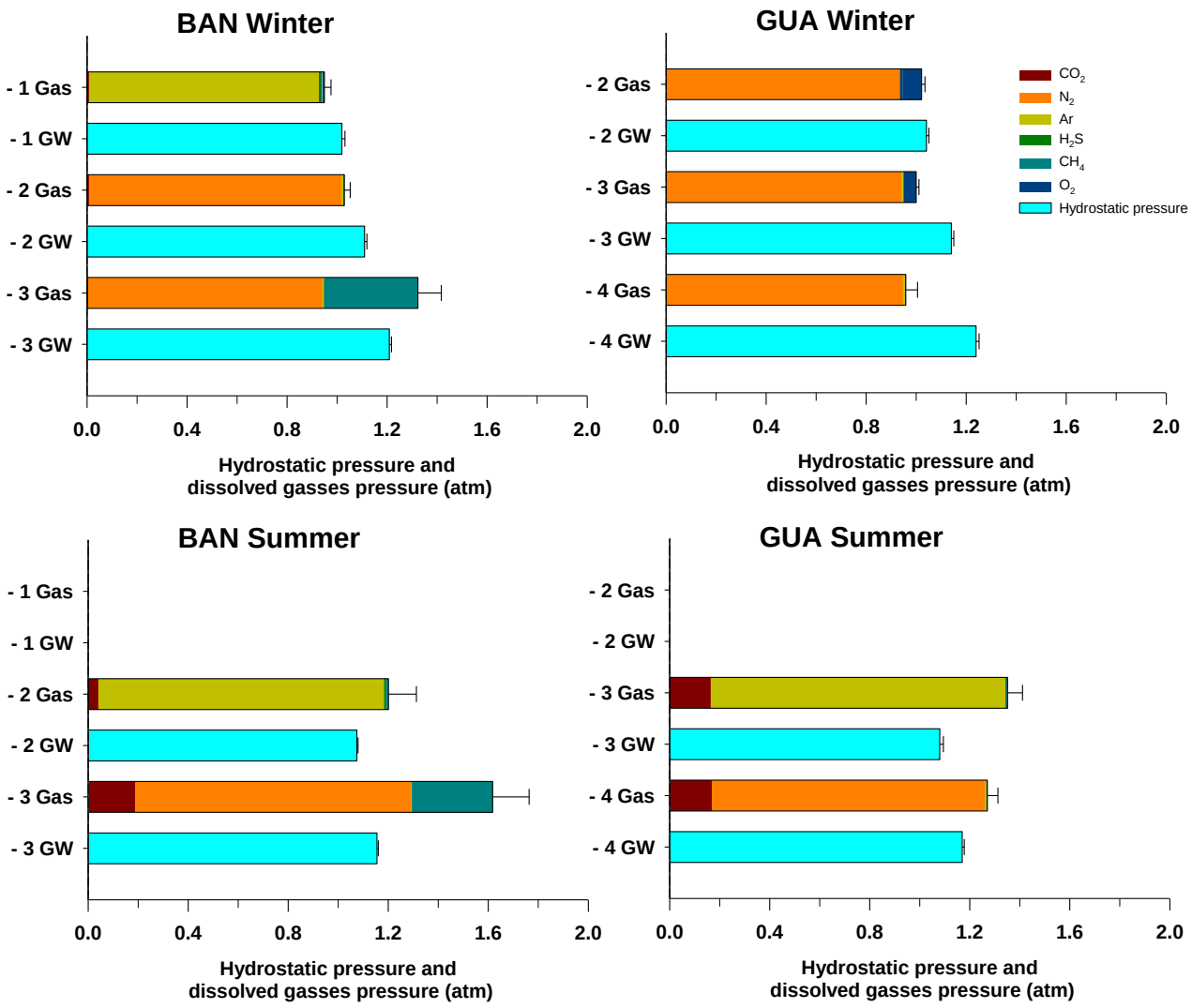

Figure 6: Partial pressure of dissolved gasses and hydrostatic pressure (atm) at BAN and GUA sites during summer (July 2017) and winter (January 2018). The error bars represent the standard deviation over 4 replicate plots. Relative gas composition is also shown using different colours in each bar.

Figure 6 shows that the dissolved gasses composition changed in summer with a marked increase of total gas pressure in all sites due to increased groundwater temperatures and thus to a decrease of effective gas solubility (see Eq. 1), considering the Bunsen coefficients. More precisely, O_2 partial pressure dropped drastically in GUA since the ORP became negative during summer (Table 2),

while CO_2 increased due to a pH decrease that in turn changed the inorganic carbon equilibrium in groundwater (Table 2). The same trend for CO_2 was also clear at BAN, but the partial pressure was always negligible since the ORP values were always extremely low, except for the months when active recharge took place.

Table 2. ORP and pH values observed in the two sites at different depths during summer (July 2017) and winter (January 2018). The standard deviation over 4 replicates is reported with the symbol ±.

Piezometer depth (m b.g.l.)	**winter**		**summer**	
	ORP (mV)	pH (-)	ORP (mV)	pH (-)
-1 at BAN	52±55	7.9±0.3		
-2 at BAN	-43±83	7.5±0.2	-192±65	6.8±0.3
-3 at BAN	-176±98	7.2±0.1	-302±29	6.9±0.1
-2 at GUA	140±50	7.0±0.7		
-3 at GUA	164±34	7.0±0.4	-105±61	7.2±0.4
-4 at GUA	87±63	6.8±0.1	-93±52	6.8±0.3

3.5. Dissolved gasses seasonal variations

The seasonal variation of dissolved gasses composition is best shown by figure 7, where the gasses that most affect the total gas pressure, to the point of exceeding the hydrostatic pressure, are shown during the entire hydrological year. At BAN, CH_4 shows the highest dissolved concentrations in spring at -3 m b.g.l., with concentrations more than one order of magnitude higher than at -2 m b.g.l.. The CH_4 concentration rapidly diminish during summer and autumn, concomitantly with the water table drawdown, suggesting CH_4 ebullition due to exsolution. The dissolved N_2 at -3 m b.g.l.

has very low concentrations in late spring and summer due to ebullition, while it reaches atmospheric values during recharge events, as also suggested by Blicher-Mathiesen et al. (1998).

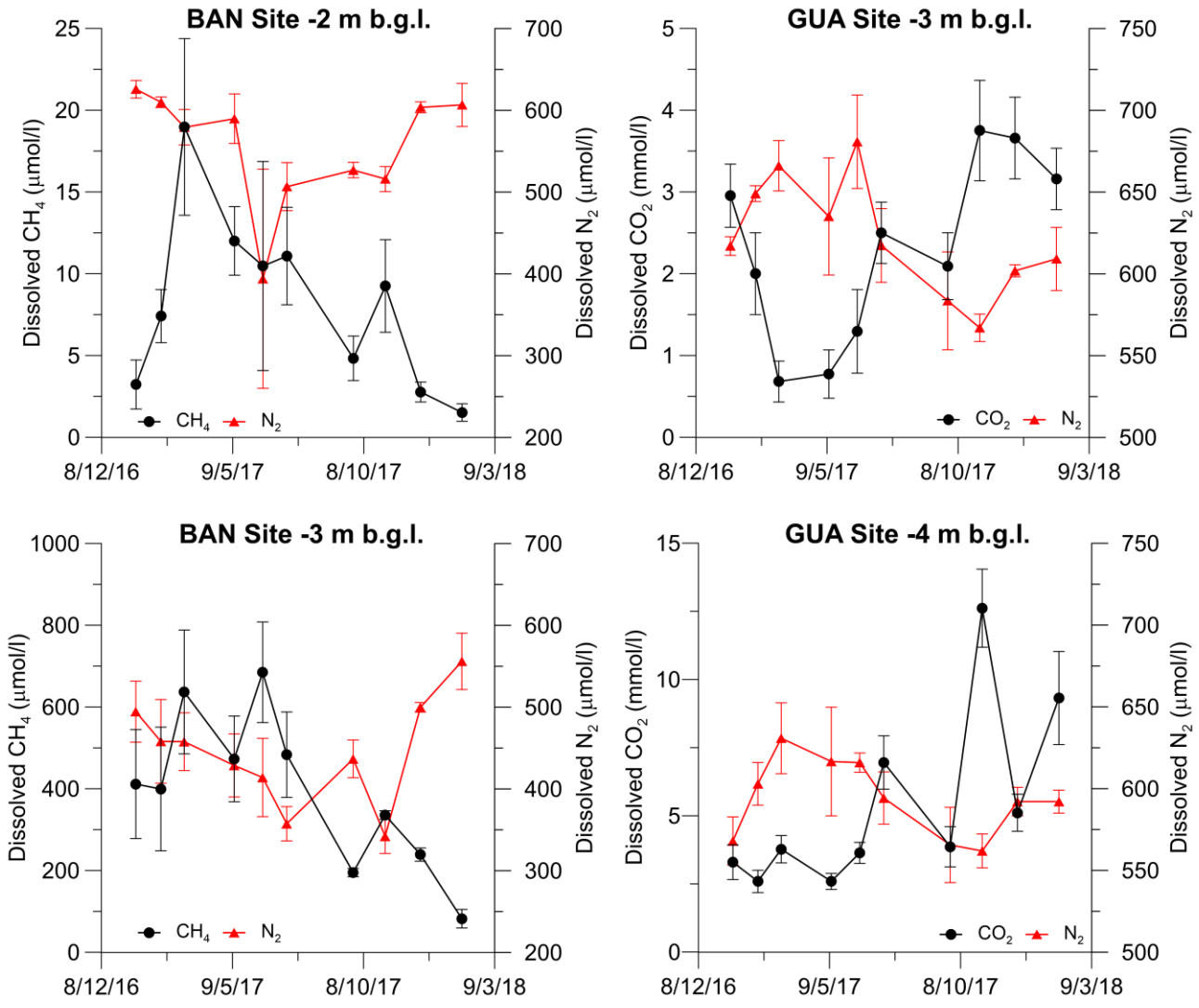

Figure 7: Dissolved gasses responsible for exsolution from groundwater (CH_4 and N_2 at BAN and CO_2 and N_2 at GUA) recorded in the MLSs at the two sites. The error bars represent the standard deviation over 4 replicate plots.

Instead, at GUA the dissolved CO_2 is increasing in summer and autumn, while N_2 is decreasing. The CO_2 increase is due to SOM oxidation processes that in turn decreased the groundwater pH (Chapelle et al., 1995). While N_2 decrease is due to lower N_2 solubility because of groundwater temperature increase and water table drawdown (Colt, 2012).

3.6. Seasonal trends of N_{2Exc} ORP and NO_3^- at GUA site

Finally, figure 8 shows the temporal evolution of N_{2Exc} calculated with the modified method M2 and compared with ORP values measured at GUA. The NO_3^- temporal evolution at GUA is also shown in figure 8 to assess if the increase of N_{2Exc} could be imputable to NO_3^- losses. The N_{2Exc} is shown only for GUA, since BAN is affected by CH_4 exsolution as previously discussed. It can be noticed that at GUA a baseline of approximately 70 µmol/l of N_{2Exc} is present during the monitoring period, while during winter and spring the N_{2Exc} reached peaks of 160 µmol/l. The ORP shows positive values indicating oxic conditions during winter, when recharge takes place. Then, it gradually decreases during spring attaining sub-oxic conditions in late summer. The ORP decrease during spring is compatible with the denitrification conditions highlighted by the N_{2Exc} increase, although NO_3^- concentrations at -3 m and -4 m b.g.l. were too low to explain the observed N_{2Exc} increase. The ORP decrease is probably due to labile substrates coming from the upper horizons and transported downward by the recharge waters (Castaldelli et al. 2013), while the decrease of N_{2Exc} after the spring peak is due to the lack of NO_3^- to further sustain denitrification. Moreover, the N_{2Exc} increase could have been generated by the denitrification at -2 m b.g.l. and transported downward by the water table drawdown (see Fig. 2). The N_{2Exc} at -2 m b.g.l. is not plotted in figure 8 since its values were always near to zero or negative (see the right plot of Fig. 5) and the ORP was always positive, suggesting that denitrification was unlikely to occur at this depth or that ebullition could impair the calculated N_{2Exc}. In fact, the hydrostatic pressure was close to the total gas pressure at -2 m b.g.l. in winter (Fig. 6).

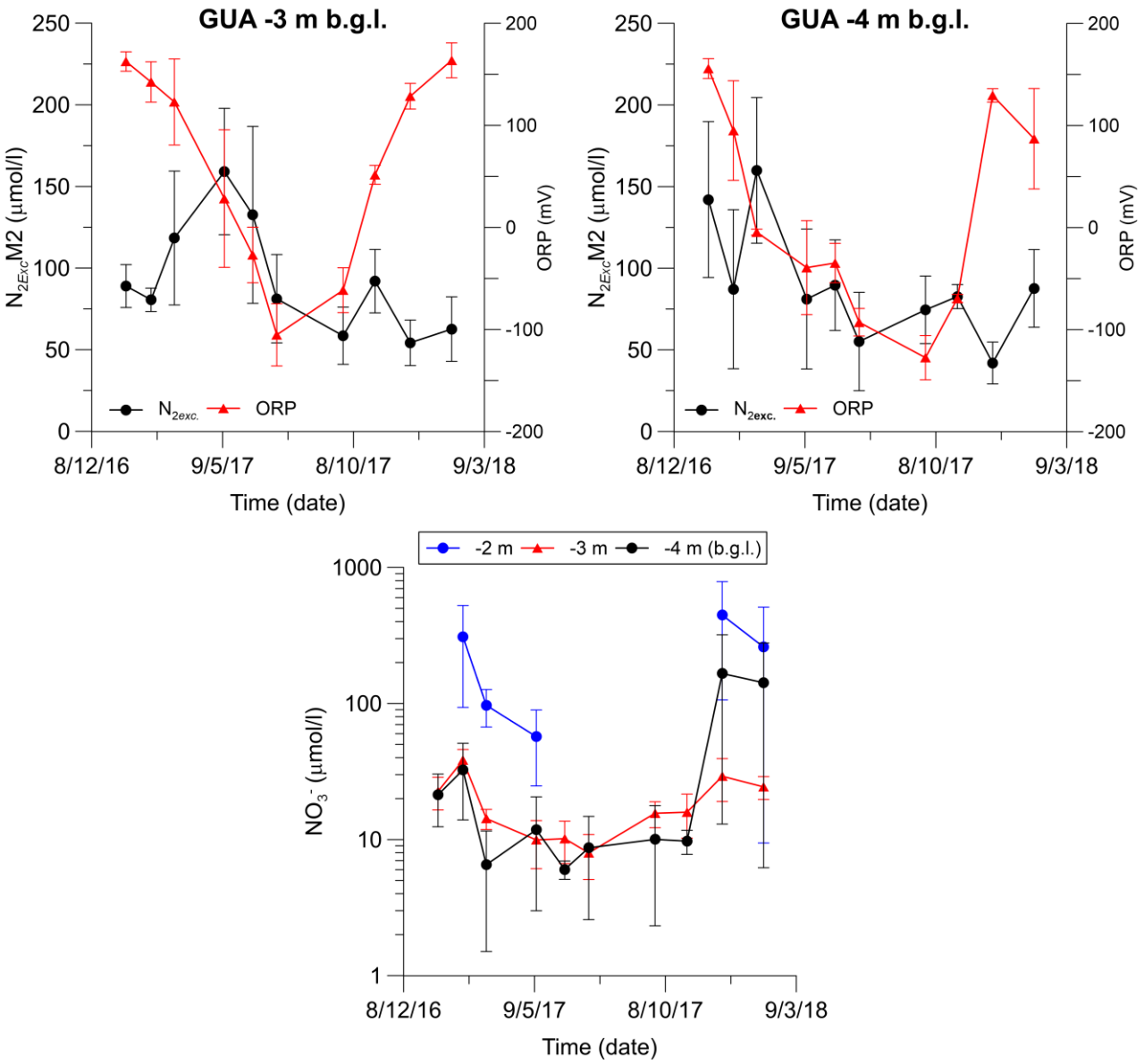

404

405 Figure 8: Temporal evolution of N_{2Exc}M2 and ORP at GUA recorded at -3 and -4 m b.g.l. (upper
406 panels). Temporal evolution of NO_3^- at GUA recorded at -2, -3 and -4 m b.g.l. (lower panel). The
407 error bars represent the standard deviation over 4 replicate plots.

408

409 In general, the N_{2Exc} here calculated for GUA agreed with the hypothesized denitrification
410 conditions, but the reacted N was low and the elevated standard deviations of both N_{2Exc} and NO_3^-
411 concentrations do not allow a clear quantification of this processes. Other physical processes like
412 mechanical dispersion and dilution with rain water poor in NO_3^- could have substantially
413 contributed to the low NO_3^- concentrations found at GUA. MLS devices resulted to be key

monitoring tools in allowing to precisely locate the sources of gasses that could trigger exsolution. In fact, exsolution processes could start in zones located far below the water table and the upward migrating gasses could change the gasses' partial pressures or even ORP and pH equilibria. All this information would be obliterated if integrated depth sampling in long screen monitoring wells were used instead of MLS devices.

4. Conclusions

This study, for the first time, reports the seasonal variations during an entire hydrological year of dissolved gasses in shallow groundwater below agricultural lands, induced by CO_2, N_2 and CH_4 exsolution. CH_4 exsolution was active only at a site where SOM was abundant due to buried peat lenses, while CO_2 and N_2 were present in both sites due to SOM oxidation, excess air and denitrification processes. N_2 was the main dissolved gas at both sites in term of partial pressure, thus small N_2 changes in concentration could largely affect the ebullition process from groundwater. Seasonal monitoring was a key issue since the water table drawdown combined with pH changes and increased temperature during summer triggered gas ebullition even in the freshwater paleo-river environment. The above-mentioned behaviour could hamper the calculation of N_2 excess also in sites where methanogenic conditions are not relevant. Besides, groundwater temperature fluctuations induced large biases in the calculated N_2 excess assuming a constant recharge temperature. This was found to be relevant even in the freshwater paleo-river environment, relatively unaffected by ebullition processes during winter, when recharge increases the hydrostatic pressure which in turn becomes higher than the total gas pressure. For these reasons, N_2 excess estimates were judged unreliable in both the investigated lowland environments using published approaches, while a modified method which accounts for the measured groundwater temperature was able to provide reliable estimates of N_2 excess at least for non-methanogenic environments. This study indicates that NO_3^- losses via denitrification estimated by N_2 excess may be significantly biased in shallow aquifers pertaining to lowland agricultural areas, since gas ebullition is the rule

rather than the exception in these environments. Future studies should be more focused to resolve the spatial and temporal variability of denitrification processes in lowland shallow aquifers agricultural by using a combination of the available electron donors, acceptors, reaction products and possibly stable isotopes.

Acknowledgments

This work was financially supported by the Emilia-Romagna Region within the Rural Development Programme (PSR) 2014-2020 and within the POR FESR 2007-2013 Programme for the development of the regional High Technology Network.

References

Aeschbach-Hertig, W., El-Gamal, H., Wieser, M., Palcsu, L., 2008. Modeling excess air and degassing in groundwater by equilibrium partitioning with a gas phase. Water Resour. Res. 44, W08449. Doi: 10.1029/2007WR006454.

Aguilera, E., Lassaletta, L., Sanz-Cobena, A., Garnier, J., Vallejo, A., 2013. The potential of organic fertilizers and water management to reduce N_2O emissions in Mediterranean climate cropping systems. A review. Agr. Ecosyst. Environ. 164, 32-52. Doi: 10.1016/j.agee.2012.09.006.

Amos, R.T., Mayer, K.U., 2006. Investigating ebullition in a sand column using dissolved gas analysis and reactive transport modeling. Environ. Sci. Technol. 40(17), 5361-5367. Doi: 10.1021/es0602501.

Anderson, T.R., Groffman, P.M., Kaushal, S.S., Walter, M.T., 2014. Shallow groundwater denitrification in riparian zones of a headwater agricultural landscape. J. Environ. Qual. 43(2), 732-744. Doi: 10.2134/jeq2013.07.0303.

Anderson, L.G., Hall, P.O., Iverfeldt, A., van der Loejf, R., Michiel, M., Sundby, B., Westerlund, S.F., 1986. Benthic respiration measured by total carbonate production. Limnol. Oceanogr. 31(2), 319-329. Doi: 10.4319/lo.1986.31.2.0319.

Barakat, M., Cheviron, B., Angulo-Jaramillo, R., 2016. Influence of the irrigation technique and strategies on the nitrogen cycle and budget: A review. Agr. Water Manage. 178, 225-238. Doi: 10.1016/j.agwat.2016.09.027.

Blicher-Mathiesen, G., McCarty, G.W., Nielsen, L.P., 1998. Denitrification and degassing in groundwater estimated from dissolved dinitrogen and argon. J. Hydrol. 208(1-2), 16-24. Doi: 10.1016/S0022-1694(98)00142-5.

Böhlke, J.K., 2002. Groundwater recharge and agricultural contamination. Hydrogeol. J. 10, 153-179. Doi: 10.1007/s10040-001-0183-3.

Bouwer H., Rice R.C., 1976. A slug test for determining hydraulic conductivity of unconfined aquifers with completely or partially penetrating wells. Water Resour. Res. 12(3), 423–428. Doi: 10.1029/WR012i003p00423.

Caschetto, M., Colombani, N., Mastrocicco, M., Petitta, M., Aravena, R., 2017. Nitrogen and sulphur cycling in the saline coastal aquifer of Ferrara, Italy. A multi-isotope approach. Appl. Geochem. 76, 88-98. Doi: 10.1016/j.apgeochem.2016.11.014.

Castaldelli, G., Colombani, N., Soana, E., Vincenzi, F., Fano, E. A., Mastrocicco, M., 2019. Reactive nitrogen losses via denitrification assessed in saturated agricultural soils. Geoderma 337, 91-98. Doi: 10.1016/j.geoderma.2018.09.018.

Castaldelli, G., Colombani, N., Vincenzi, F., Mastrocicco, M., 2013. Linking dissolved organic carbon, acetate and denitrification in agricultural soils. Environ. Earth Sci. 68(4), 939-945. Doi: 10.1007/s12665-012-1796-7.

Cey, B.D., Hudson, G.B., Moran, J.E., Scanlon, B.R., 2009. Evaluation of noble gas recharge temperatures in a shallow unconfined aquifer. Groundwater 47(5), 646-659. Doi: 10.1111/j.1745-6584.2009.00562.x.

Chapelle, F.H., McMahon, P.B., Dubrovsky, N.M., Fujii, R.F., Oaksford, E.T., Vroblesky, D.A., 1995. Deducing the distribution of terminal electron-accepting processes in hydrologically diverse groundwater systems. Water Resour. Res. 31(2), 359-371. Doi: 10.1029/94WR02525.

Chen, S., Wang, F., Zhang, Y., Qin, S., Wei, S., Wang, S., Hu, C., Liu, B., 2018. Organic carbon availability limiting microbial denitrification in the deep vadose zone. Environ. Microbiol. 20(3), 980-992. Doi: 10.1111/1462-2920.14027.

Cline, J.D., 1969. Spectrophotometric determination of hydrogen sulfide in natural waters 1. Limnol. Oceanogr. 14(3), 454-458. Doi: 10.4319/lo.1969.14.3.0454.

514 Colombani, N., Di Giuseppe, D., Faccini, B., Ferretti, G., Mastrocicco, M., Coltorti, M., 2016a.
515 Inferring the interconnections between surface water bodies, tile-drains and an unconfined aquifer–
516 aquitard system: a case study. J. Hydrol. 537, 86-95. Doi: 10.1016/j.jhydrol.2016.03.046.
517
518 Colombani, N., Giambastiani, B.M.S., Mastrocicco, M., 2016b. Use of shallow groundwater
519 temperature profiles to infer climate and land use change: interpretation and measurement
520 challenges. Hydrol. Proc. 30(14), 2512-2524. Doi: 10.1002/hyp.10805.
521
522 Colt, J., 2012. Solubility of atmospheric gases in brackish and marine waters, in: Dissolved Gas
523 Concentration in Water Computation as Functions of Temperature, Salinity and Pressure, 2nd Ed.
524 Elsevier, London, pp. 73-131. Doi: 10.1016/C2011-0-06095-7.
525
526 Denver, J.M., Ator, S.W., Lang, M.W., Fisher, T.R., Gustafson, A.B., Fox, R., Clune, J.W.,
527 McCarty, G.W., 2014. Nitrate fate and transport through current and former depressional wetlands
528 in an agricultural landscape, Choptank Watershed, Maryland, United States. J. Soil Water Conserv.
529 69(1), 1-16. Doi: 10.2489/jswc.69.1.1.
530
531 Fortuin, N.P., Willemsen, A., 2005. Exsolution of nitrogen and argon by methanogenesis in Dutch
532 ground water. J. Hydrol. 301(1-4), 1-13. Doi: 10.1016/j.jhydrol.2004.06.018.
533
534 Fox, R.J., Fisher, T.R., Gustafson, A.B., Jordan, T.E., Kana, T.M., Lang, M.W., 2014. Searching for
535 the missing nitrogen: biogenic nitrogen gases in groundwater and streams. J. Agr. Sci. 152(S1), 96-
536 106. Doi: 10.1017/S0021859614000070.
537

538 Greggio, N., Giambastiani, B.M.S., Campo, B., Dinelli, E., Amorosi, A., 2018. Sediment
539 composition, provenance, and Holocene paleoenvironmental evolution of the Southern Po River
540 coastal plain (Italy). Geol. J. 53(3), 914-928. Doi: 10.1002/gj.2934.
541
542 Holocher, J., Peeters, F., Aeschbach-Hertig, W., Hofer, M., Brennwald, M., Kinzelbach, W., Kipfer,
543 R., 2002. Experimental investigations on the formation of excess air in quasi-saturated porous
544 media. Geoch. Cosm. Acta 66, 4103–4117. Doi: 10.1016/S0016-7037(02)00992-4.
545
546 Klump, S., Cirpka, O.A., Surbeck, H., Kipfer, R., 2008. Experimental and numerical studies on
547 excess-air formation in quasi-saturated porous media. Water Resour. Res. 44(5), W05402. Doi:
548 10.1029/2007WR006280.
549
550 Kurylyk, B.L., MacQuarrie, K.T., Voss, C.I., 2014. Climate change impacts on the temperature and
551 magnitude of groundwater discharge from shallow, unconfined aquifers. Water Resour. Res. 50(4),
552 3253-3274. Doi: 10.1002/2013WR014588.
553
554 Mastrocicco, M., Di Giuseppe, D., Vincenzi, F., Colombani, N., Castaldelli, G., 2017. Chlorate
555 origin and fate in shallow groundwater below agricultural landscapes. Environ. Pollut. 231, 1453-
556 1462. Doi: 10.1016/j.envpol.2017.09.007.
557
558 Mastrocicco, M., Colombani, N., Palpacelli, S., Castaldelli, G., 2011a. Large tank experiment on
559 nitrate fate and transport: the role of permeability distribution. Environ. Earth Sci. 63(5), 903-914.
560 Doi: 10.1007/s12665-010-0759-0.
561

562 Mastrocicco, M., Colombani, N., Salemi, E., Castaldelli, G., 2011b. Reactive modeling of
563 denitrification in soils with natural and depleted organic matter. Water, Air, Soil Pollut. 222(1-4),
564 205-215. Doi: 10.1007/s11270-011-0817-6.
565
566 Mastrocicco, M., Colombani, N., Salemi, E., Castaldelli, G., 2010. Numerical assessment of
567 effective evapotranspiration from maize plots to estimate groundwater recharge in lowlands. Agr.
568 Water Manage. 97(9), 1389-1398. Doi: 10.1016/j.agwat.2010.04.005.
569
570 Parkhurst, D.L., Appelo, C.A.J., 2013. Description of input and examples for PHREEQC version 3-
571 A computer program for speciation, batch-reaction, one-dimensional transport, and inverse
572 geochemical calculations. U.S. Geological Survey Techniques and Methods, book 6, chap. A43,
573 497 p., available at https://pubs.usgs.gov/tm/06/a43.
574
575 Rivett, M.O., Buss, S.R., Morgan, P., Smith, J.W., Bemment, C.D., 2008. Nitrate attenuation in
576 groundwater: a review of biogeochemical controlling processes. Water Res. 42(16), 4215-4232.
577 Doi: 10.1016/j.watres.2008.07.020.
578
579 Sacchi, E., Acutis, M., Bartoli, M., Brenna, S., Delconte, C.A., Laini, A., Pennisi, M., 2013. Origin
580 and fate of nitrates in groundwater from the central Po plain: insights from isotopic investigations.
581 Appl. Geochem. 34, 164-180. Doi: 10.1016/j.apgeochem.2013.03.008.
582
583 Starr, R.C., Gillham, R.W., 1993. Denitrification and organic carbon availability in two aquifers.
584 Groundwater 31(6), 934-947. Doi: 10.1111/j.1745-6584.1993.tb00867.x.
585
586 Taylor, P.G., Townsend, A.R., 2010. Stoichiometric control of organic carbon–nitrate relationships
587 from soils to the sea. Nature 464(7292), 1178-1181. Doi: 10.1038/nature08985.

588

589 Tesoriero, A.J., Liebscher, H., Cox, S.E., 2000. Mechanism and rate of denitrification in an
590 agricultural watershed: Electron and mass balance along groundwater flow paths. Water Resour.
591 Res. 36(6), 1545-1559. Doi: 10.1029/2000WR900035.

592

593 Vepraskas, M.J., 2015. History of the Concept of Hydric Soil, in Vepraskas M.J., Craft C.B. (Eds),
594 Wetland Soils: Genesis, Hydrology, Landscapes and Classification. CRC Press, Boca Raton, pp.
595 23-38. Doi: 10.1201/b18996-4.

596

597 Vogel, J.C., Talma, A.S., Heaton, T.H.E., 1981. Gaseous nitrogen as evidence for denitrification in
598 groundwater. J. Hydrol. 50, 191-200. Doi: 10.1016/0022-1694(81)90069-X.

599

600 Ward, A., Sharpley, A., Miller, K., Dick, W., Hoorman, J., Fulton, J., LaBarge, G.A., 2018. An
601 assessment of in-field nutrient best management practices for agricultural crop systems with
602 subsurface drainage. J. Soil Water Conserv. 73(1), 5A-10A. Doi: 10.2489/jswc.73.1.5A.

603

604 Weymann, D., Well, R., Flessa, H., Heide, C.V.D., Deurer, M., Meyer, K., Konrad, C., Walther,
605 W., 2008. Groundwater N_2O emission factors of nitrate-contaminated aquifers as derived from
606 denitrification progress and N_2O accumulation. Biogeosci. 5(5), 1215-1226. Doi: 10.5194/bg-5-
607 1215-2008.

608